Final Report: Investigation of Polarization Spectroscopy and Degenerate Four-Wave Mixing for Quantitative Concentration Measurements

Grant No. DE-FG03-99ER14997 (Texas A&M University), May 1, 2001–February 28, 2003

Principal Investigator: Robert P. Lucht (Lucht@purdue.edu)
School of Mechanical Engineering, Purdue University, West Lafayette, Indiana 47907-2088

Graduate Students Supported: Sukesh Roy, Sherif Hanna, and Waruna Kulatilaka

I. PROGRAM SCOPE

Laser-induced polarization spectroscopy (LIPS), degenerate four-wave mixing (DFWM), and electronic-resonance-enhanced (ERE) coherent anti-Stokes Raman scattering (CARS) are techniques that shows great promise for sensitive measurements of transient gas-phase species, and diagnostic applications of these techniques are being pursued actively at laboratories throughout the world. However, significant questions remain regarding strategies for quantitative concentration measurements using these techniques. The primary objective of this research program is to develop and test strategies for quantitative concentration measurements in flames and plasmas using these nonlinear optical techniques. Theoretically, we are investigating the physics of these processes by direct numerical integration (DNI) of the time-dependent density matrix equations that describe the wave-mixing interaction. Significantly fewer restrictive assumptions are required when the density matrix equations are solved using this DNI approach compared with the assumptions required to obtain analytical solutions. For example, for LIPS calculations, the Zeeman state structure and hyperfine structure of the resonance and effects such as Doppler broadening can be included. There is no restriction on the intensity of the pump and probe beams in these nonperturbative calculations, and both the pump and probe beam intensities can be high enough to saturate the resonance. As computer processing speeds have increased, we have incorporated more complicated physical models into our DNI codes. During the last project period we developed numerical methods for nonperturbative calculations of the two-photon absorption process.

Experimentally, diagnostic techniques are developed and demonstrated in gas cells and/or well-characterized flames for ease of comparison with model results. The techniques of two-photon, two-color H-atom LIPS and three-laser ERE CARS for NO and C_2H_2 were demonstrated during the project period, and nonperturbative numerical models of both of these techniques were developed. In addition, we developed new single-mode, injection-seeded optical parametric laser sources (OPLSs) that will be used to replace multi-mode commercial dye lasers in our experimental measurements. The use of single-mode laser radiation in our experiments will increase significantly the rigor with which theory and experiment are compared.

II. THEORETICAL AND EXPERIMENTAL INVESTIGATION OF LASER-INDUCED POLARIZATION SPECTROSCOPY (LIPS)

Theoretical Analysis of Two-Photon, Two-Color LIPS

The physics of two-color laser-induced polarization spectroscopy (LIPS) of the hydrogen atom is being investigated by numerical solution of the time-dependent density matrix equations.
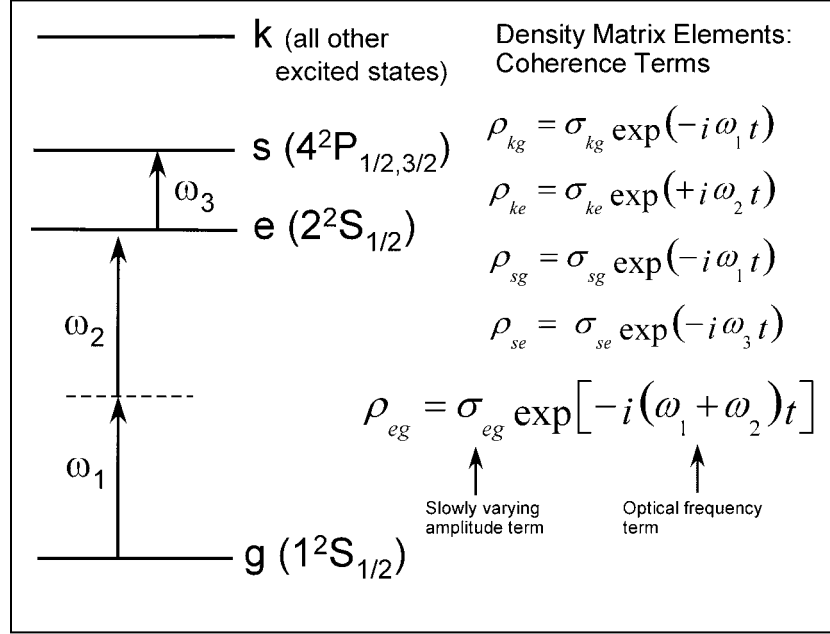
The pump beam ($\omega_1 = \omega_2$) for the two-color LIPS process is tuned to the two-photon $1^2S_{1/2}$–$2^2S_{1/2}$ of the H atom, as illustrated in Fig. 1. The two-photon absorption process for the $1^2S_{1/2}$–$2^2S_{1/2}$ transition proceeds through the $n^2P_{1/2}$ and $n^2P_{3/2}$ levels, where $n \geq 2$, which are coupled with the $1^2S_{1/2}$ and $2^2S_{1/2}$ levels by single-photon resonances. The two-photon absorption process is treated in a nonperturbative fashion in the numerical analysis. The coherence density matrix elements for the single-photon resonances between the n^2P levels and either the $1^2S_{1/2}$ or $2^2S_{1/2}$ levels are assumed to be given by the steady state solution of the appropriate density matrix equation. The probe beam at frequency ω_3 is tuned to the single-photon $2^2S_{1/2}$–$4^2P_{1/2,3/2}$ resonance. The hyperfine structure of the H-atom energy levels is incl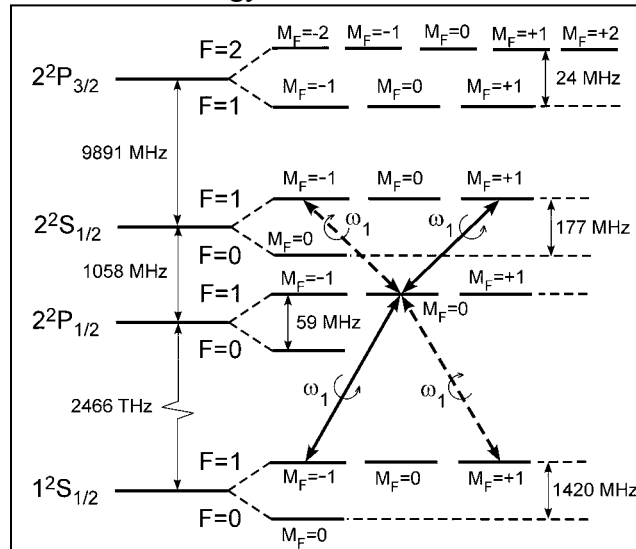uded in the analysis, and the Zeeman states are included, as shown in Fig. 2, so that effects of the polarization properties of the laser fields are treated in a rigorous fashion. A total of 92 quantum states are included in the numerical simulation. In Fig. 2, we show the two-photon process proceeding through the intermediate $2^2P_{1/2}$ level. We found from our numerical analysis that saturation and Stark shifting of the two-photon interaction $1^2S_{1/2}$–$2^2S_{1/2}$ transition is dominated by the $2^2P_{1/2}$ and $2^2P_{3/2}$ intermediate levels. In previous studies this level was not included in the calculation of the two-photon cross-section [1]. We have investigated the effects of saturation on the two-photon resonance in detail. A paper describing the numerical analysis is in preparation for submission to the Journal of Chemical Physics.
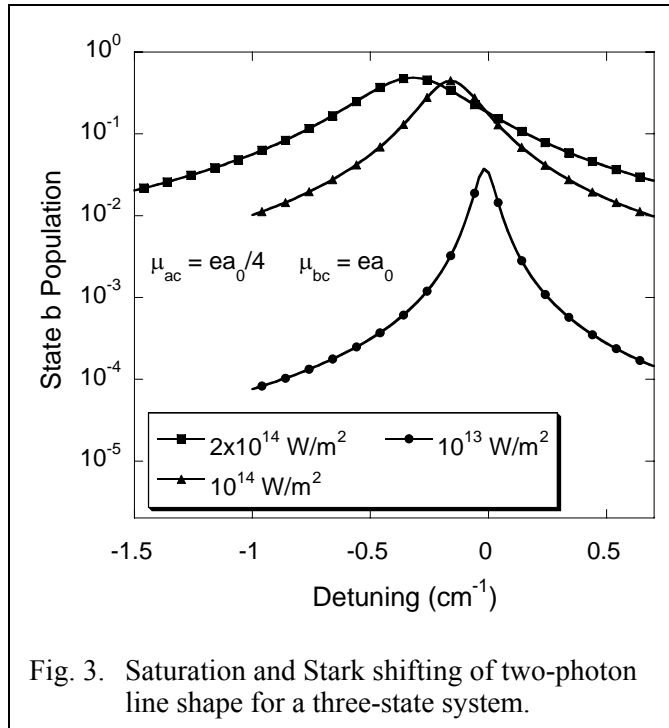

Fig. 2. Detailed quantum state structure for DNI analysis of two-photon, two-color H-atom LIPS.

Fig. 3. Saturation and Stark shifting of two-photon line shape for a three-state system.
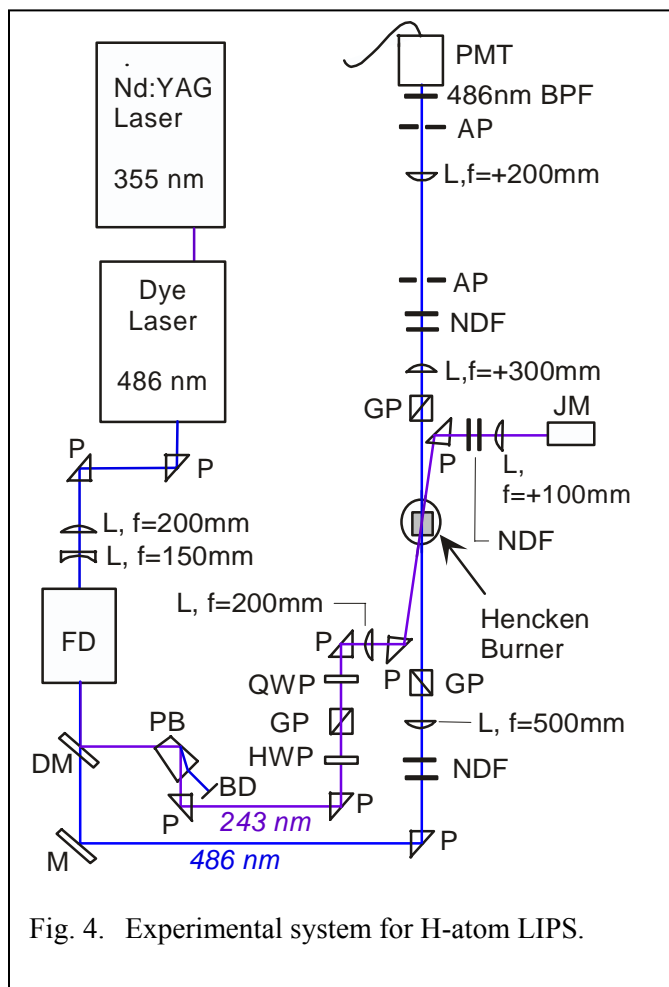

Fig. 4. Experimental system for H-atom LIPS.

The development of numerical methods for the evaluation of two-photon absorption line shapes, saturation, and Stark shifting was needed for analysis of the LIPS process, but we have also worked on simpler model to gain physical insight. We have solved the steady state density matrix equations for a three-state system (a = ground state, b = final state, c = intermediate state) to obtain further insight into the physics of the two-photon absorption process. The line shapes for the three-state system that approximates the H-atom $1^2S_{1/2}$–$2^2S_{1/2}$ two-photon-transition with a $2^2P_{1/2,3/2}$ intermediate level are shown in Fig. 3. The saturation and Stark shifting of the two-photon resonance line is clearly visible. We have developed an analytical expression for the

Stark shift and discovered that the direction of the Stark shift is determined by the relative magnitudes of the dipole moments μ_{ac} and μ_{bc}, at least for the case where the pump laser frequency is far from resonance with the single-photon ac and bc resonances. A paper describing the three-state analysis is in preparation for submission to Optics Communications.

Laser-Induced Polarization Spectroscopy Measurements of H-atoms in Flames

Two-color, two-photon laser-induced polarization spectroscopy (LIPS) of atomic hydrogen was demonstrated and applied in atmospheric pressure hydrogen/air flames [2] and in low-pressure C_2H_2/O_2 flames. The experimental system for the LIPS measurements is depicted schematically in Fig. 4. Fundamental and frequency-doubled beams from a single 486-nm dye laser were used in the experiments. The 243-nm pump beam in the measurements was tuned to the two-photon $1^2S_{1/2}$–$2^2S_{1/2}$ resonance of the hydrogen atom. The 486-nm probe beam was tuned to the
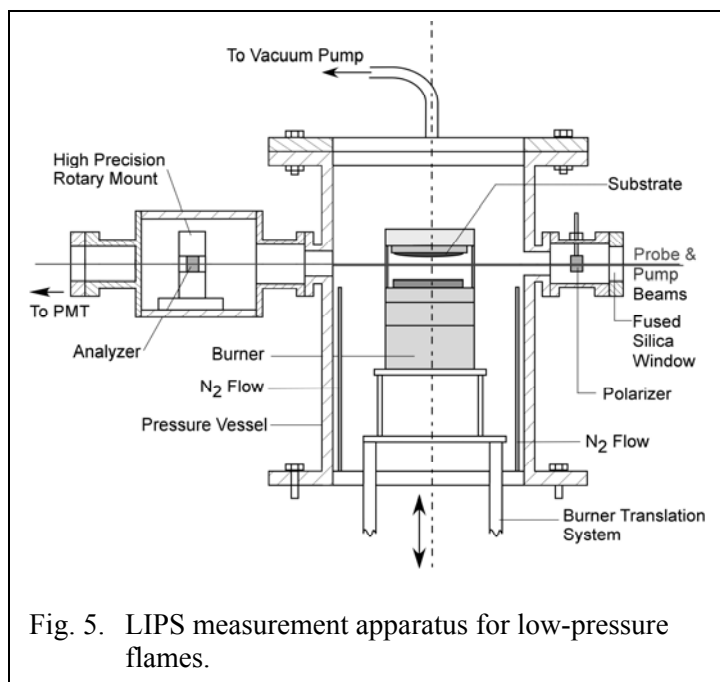
Fig. 5. LIPS measurement apparatus for low-pressure flames.

single-photon $2^2S_{1/2}$–$4^2P_{1/2,3/2}$ resonance of the hydrogen atom. Measurements were performed in an atmospheric pressure H_2/air flame stabilized on a near-adiabatic, flat-flame calibration burner (Kulatilaka et al., 2004a). For the range of pump beam intensities used, the LIPS signal in the atmospheric pressure flame was found to be nearly proportional to the square of the pump beam intensity over a wide range of flame equivalence ratios. Spectral line shapes were recorded at flame equivalence ratios ranging from 0.85 to 2.10. Horizontal and vertical H-atom number density distribution profiles were measured in the Hencken burner. The vertical H-atom number density profiles measured along the burner centerline for various flame equivalence ratios were compared with the results of a numerical flame calculation using the UNICORN (UNsteady Ignition and COmbustion with ReactioNs) code. Good agreement between theory and experiment was obtained for stoichiometric and rich flame conditions.

A modification of the low-pressure flame system was necessary to perform the LIPS measurements; the crossed polarizers for the probe beams were located inside the pressure vessel windows, as shown in Fig. 5, to avoid signal degradation due to window birefringence. The results of H-atom profile measurements in the low-pressure C_2H_2/O_2 flames are shown in Fig. 6
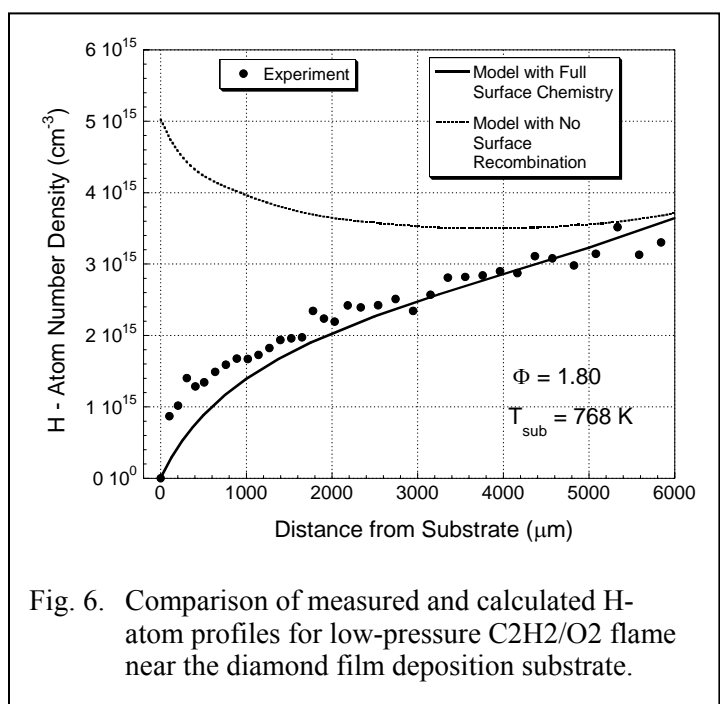

Fig. 6. Comparison of measured and calculated H-atom profiles for low-pressure C2H2/O2 flame near the diamond film deposition substrate.

for a flame with an equivalence ratio of 1.80. The profile is in excellent agreement with a numerical flame simulation including full surface chemistry. These flames were operated at diamond-forming conditions, and previous attempts to detect the H-atom in these flames by three-photon-induced LIF were completely unsuccessful. However, two-photon, two-color LIPS signals were quite high and measurements were performed successfully to within 25 μm of the deposition surface. A paper describing these measurements is in preparation for submission to Combustion and Flame.

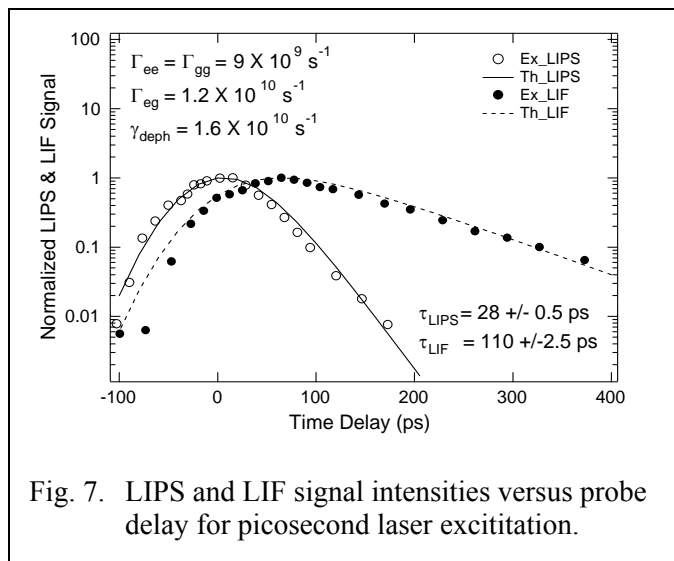H-atom LIPS measurements were also performed in the Picosecond

Fig. 7. LIPS and LIF signal intensities versus probe delay for picosecond laser excititation.

Laser Facility at Sandia National Laboratories in Livermore, California in collaboration with Tom Settersten (Sandia), Sukesh Roy (ISSI, Dayton, Ohio), and Jim Gord (AFRL, Wright-Patterson Air Force Base (Roy et al., 2004) [3]. In these experiments the line shape was recorded at several different laser powers. Saturation broadening and Stark shifting of the two-photon $1^2S_{1/2}$–$2^2S_{1/2}$ resonance was observed at intensity levels that were in good agreement with DNI calculations of the LIPS process. In addition, the 486-nm probe beam was delayed with respect to the 243-nm pump beam using a computer controlled translation stage. Both the two-photon, two-color LIPS and LIF signals were recorded as a function of probe delay time. The results of these measurements are shown in Fig. 7. The solid lines in Fig. 7 are the results of DNI calculations using the 92-state simulation discussed in the previous section. Because of the simultaneous recording of both the LIF and LIPS signals, both the collisional quenching rate from 2S and 2P levels and the rate of collisional transfer between Zeeman levels in the 2S and 2P levels can be determined by comparing theory and experiment.

Polarization Effects in OH LIPS Measurements

A series of measurements on the effect of the pump polarization on the LIPS signal for OH in atmospheric pressure flames was performed. These measurements were performed over a wide range of laser powers for different types of OH rotational transitions. The LIPS signal was recorded as the pump polarization was varied from linear to circular with a quarter-wave plate. The experimental measurements are compared with the results of DNI numerical modeling that includes the hyperfine structure of the OH molecule. This comparison is still in progress.
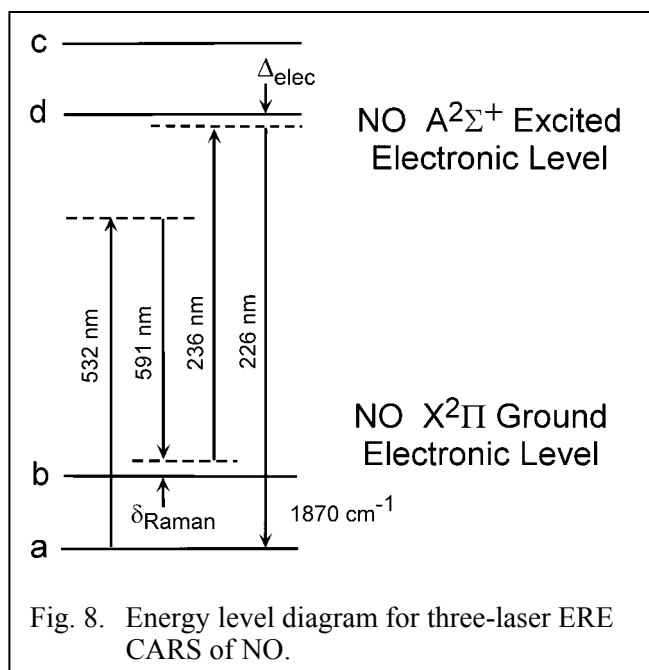
III. THEORETICAL AND EXPERIMENTAL INVESTIGATION OF ELECTRONIC-RESONANCE-ENHANCED (ERE) COHERENT ANTI-STOKES RAMAN SCATTERING (CARS)

ERE CARS Measurements of NO and C_2H_2

Electronic-resonance-enhanced (ERE) coherent anti-Stokes Raman scattering (CARS) measurements of nitric oxide (NO) and C_2H_2 were performed using a three-laser CARS technique [4]. An energy level schematic for the NO ERE CARS process is shown in Fig. 8. The first pump and the Stokes beam are visible laser beams with frequencies far from resonance with the $A^2\Sigma^+$ - $X^2\Pi$ electronic transition. The probe beam at frequency ω_3 is at or near electronic resonance. This wide separation of the frequencies ω_1 and ω_3 of the two pump beams distinguishes our technique from previous ERE CARS experiments, which were performed with the same laser frequency for the pump and probe beams, and with all three beams at or near electronic resonance.

The pump source for the ω_1 pump beam was a Continuum Model 9010 injection-seeded, Q-switched Nd:YAG laser with a repetition rate of 10 Hz, pulse length of approximately 7 ns, and pulse energy for the 532-nm output of approximately 750 mJ. The 532-nm output was also used to pump a Continuum Model ND6000 narrowband, tunable dye laser to produce the Stokes beam (ω_2) at a wavelength near 590 nm with a frequency bandwidth of approximately 0.08 cm^{-1}. The 355-nm third-harmonic output of a Continuum Model 8010 Nd:YAG laser was used to pump a second Continuum Model ND6000 dye laser to produce tunable laser radiation at a wavelength of 472 nm. The 472-nm output of the dye laser was frequency-doubled to 236 nm to produce the probe beam at frequency ω_3 with an estimated frequency bandwidth of 0.2-0.3 cm^{-1}.

Fig. 8.   Energy level diagram for three-laser ERE CARS of NO.

The CARS signal was generated using a three-dimensionally phase-matched arrangement. The ERE CARS signal was directed through apertures and four 45°-incidence, 215-nm dielectric mirrors. The 215-nm mirrors were used at 0° incidence and had approximately 70% transmittance at 226 nm but less than 1% transmittance at 236-nm. These mirrors served as spectral filters and reduced significantly the background from the 236-nm scattered light. The ERE CARS signal beam was then focused onto the entrance slit of a SPEX 0.5-m spectrometer, and a Hamamatsu Model R166 solar-blind-photomultiplier was used to detect the 226-nm ERE CARS signal. Polarization techniques were used to suppress the nonresonant four-wave mixing background signal.
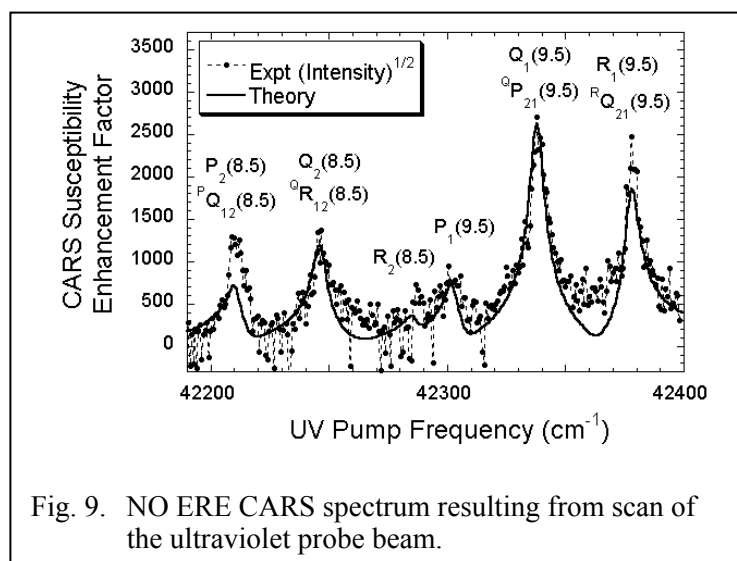
The results of a spectral scan of the ultraviolet pump beam frequency ω_3 at fixed Raman shift $\omega_1 - \omega_2$ is shown in Fig. 9. The scan was performed on a mixture of 1000 ppm of NO in a buffer gas of N_2. The cell was at room temperature, approximately 300 K, and at a pressure of 13.0 kPa (100 Torr). The spectrum was modeled using a perturbative ERE CARS analysis.

Fig. 9.   NO ERE CARS spectrum resulting from scan of the ultraviolet probe beam.

The basic equation for the CARS susceptibility is given by

$$\chi_{CARS}\left(\omega_4:\omega_1,-\omega_2,\omega_3\right) = \frac{N}{\hbar^3}\sum_{a,b,c,d}\left\{\left[\frac{1}{\omega_{ba}-\left(\omega_1-\omega_2\right)-i\Gamma_{ba}}\right]\left[\frac{\mu_{4ad}\mu_{3db}}{\omega_{da}-\omega_4-i\Gamma_{da}}\right]\right.$$

$$\left. \times \left[\left(\frac{\rho_{aa}^{(0)}\mu_{1bc}\mu_{2ca}}{\omega_{ca}+\omega_2-i\Gamma_{ca}}\right)+\left(\frac{\rho_{aa}^{(0)}\mu_{2bc}\mu_{1ca}}{\omega_{ca}-\omega_1-i\Gamma_{ca}}\right)-\left(\frac{\rho_{bb}^{(0)}\mu_{2bc}\mu_{1ca}}{\omega_{cb}-\omega_2+i\Gamma_{cb}}\right)-\left(\frac{\rho_{bb}^{(0)}\mu_{1bc}\mu_{2ca}}{\omega_{cb}+\omega_1+i\Gamma_{cb}}\right)\right]\right\}$$

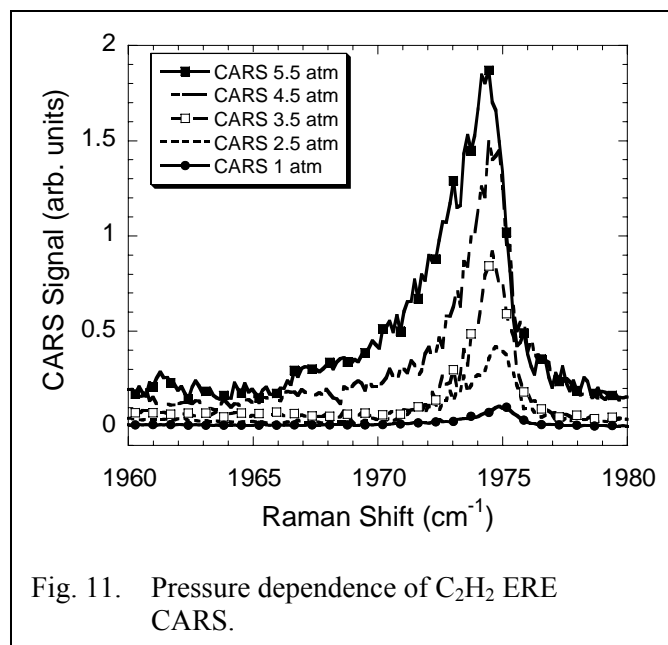where $\chi_{CARS}\left(\omega_4:\omega_1,-\omega_2,\omega_3\right)$ is the CARS susceptibility, $\mu_{1ac}=\vec{\mu}_{ac}\cdot\hat{e}_1$, where $\vec{\mu}_{ac}$ (C-m) is the electric dipole moment matrix element for states a and c, and $\hat{e}_1$ is the unit polarization vector for the electric field of pump 1, $\rho_{aa}^{(0)}$ is the initial population of state a, N is the total number density (m^{-3}) of resonant molecules, $\hbar$ is Planck's constant (J-s), Γ_{ab} is the dephasing rate (s^{-1}) for the electric dipole transition between states a and b, and other parameters are defined in a similar fashion. The square root of the CARS intensity is plotted in Fig. 9 versus the theoretical enhancement factor. The enhancement factor is the square root of the calculated CARS intensity for the ultraviolet pump frequency divided by square root of the calculated CARS intensity for λ_3 = 532 nm. There is good agreement between theory and experiment and we observe an enhancement factor of nearly 2500 at the peak of the $Q_1(9.5)$ line. The spectral line assignments in Fig. 9 can be understood by examination of Fig. 10. The main-branch electronic resonances, $Q_1(9.5)$, $R_1(9.5)$, and $P_1(9.5)$ will be predominant in the spectrum when the Raman Q-branch transition between the $J = 9.5 = N+0.5$ levels in the (1,0) band in the $X^2\Pi$ state is probed. The occurrence of the $Q_2(8.5)$, $R_2(8.5)$, and $P_2(8.5)$ lines in the same scan indicates that the Raman Q-branch transition between the $J = 8.5 = N-0.5$ levels in the (1,0) band occurs at nearly the same Raman shift.

There appears to be significant saturation of the ultraviolet transition, because it was necessary to increase the spectral width of the ultraviolet pump laser to a value of 6 cm^{-1} to obtain good agreement between the experimental and theoretical width of the resonance lines. This increase in ultraviolet pump spectral width decreased the theoretical susceptibility enhancement factor by more than a factor of 10. Good agreement between theory and experiment was also achieved for spectra obtained when the Stokes laser was scanned. Signal-to-noise ratios in excess of 10 were obtained from mixtures of 100 ppm NO in N_2 buffer gas.
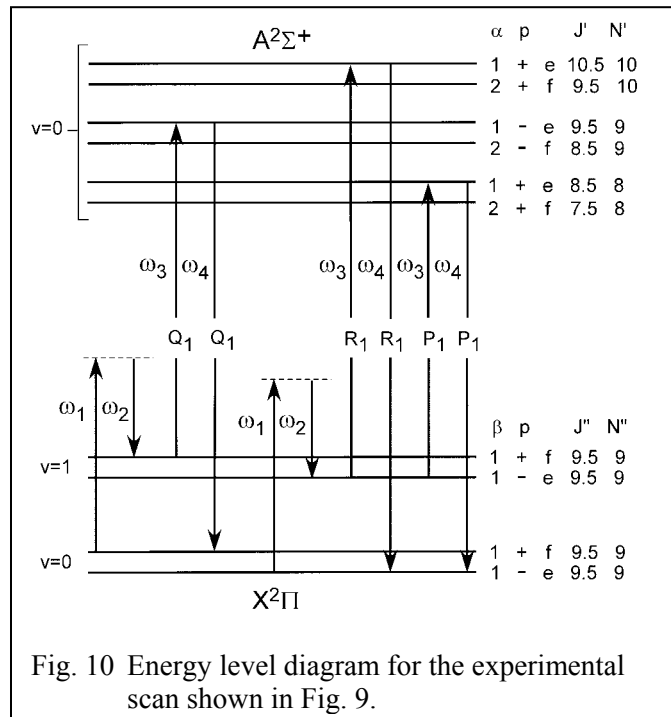
ERE CARS measurements of acetylene were also performed with an experimental set-up very similar to that for NO. The experiments were performed on a gas mixture of 5000 ppm of C_2H_2 in a buffer gas of N_2. The results of a study of

Fig. 10 Energy level diagram for the experimental scan shown in Fig. 9.

Fig. 11.   Pressure dependence of C_2H_2 ERE CARS.

the pressure dependence of the C_2H_2 ERE CARS signal are shown in Fig. 11. Analysis of the data shown in Fig. 11 reveals that the ERE CARS signal increases as the square of the pressure; this is an extremely encouraging result for ERE CARS. For LIF, the signal decreases slightly as pressure increases for constant mole fraction of a fluorescing species such as NO owing to the broadening of the excitation transition and the increase in the quenching rate with increasing pressure. A paper describing the three-acetylene ERE CARS study is in preparation for submission to Applied Physics B.

DNI Modeling of ERE CARS

The time-dependent density matrix equations that describe the ERE CARS process have been derived and a DNI numerical code for the analysis of the NO ERE CARS process has been developed. We have used this code to confirm that significant saturation of the ultraviolet electronic transitions of NO occurred at the probe beam intensities that were used in the experiment. The structure of the code is very similar to the structure of the DNI code for analysis of two-photon, two-color LIPS. Some preliminary calculations were performed with this code, and detailed plans for further code development are included in the proposal.

IV. DEVELOPMENT AND CHARACTERIZATION OF SINGLE-MODE, TUNABLE OPTICAL PARAMETRIC LASER SOURCES

We have developed and demonstrated an injection-seeded optical parametric laser source (OPLS) system for high-resolution spectroscopy and laser diagnostic measurements [5]. The OPLS is based on 355-nm pumping of nonlinear beta barium borate (β-BBO) crystals. The OPLS system is seeded using a near-infrared distributed feedback (DFB) diode laser system. The development of a compact, affordable laser source for the generation of tunable, high-resolution pulsed radiation over a wide range of wavelengths will be a major step forward in combustion diagnostics. Typically, commercial Nd:YAG-pumped dye lasers or optical parametric oscillators are used for combustion diagnostic techniques such as absorption spectroscopy, cavity ring-down spectroscopy (CRDS), LIF, LIPS, and DFWM. These commercial sources typically have frequency bandwidths on the order of 0.1 cm^{-1} (3 GHz) are exhibit multiple longitudinal frequency modes. The use of these multi-longitudinal-mode laser sources can cause numerous complications in signal analysis and greatly increase pulse-to-pulse signal fluctuations in techniques such as LIPS [6] and CRDS [7].

The basis for the operation of our OPLS systems is the observation that we can obtain a significant enhancement of the signal and idler intensities in a single β-BBO crystal when the optical parametric process is initiated using a DFB diode laser at the idler wavelength. The

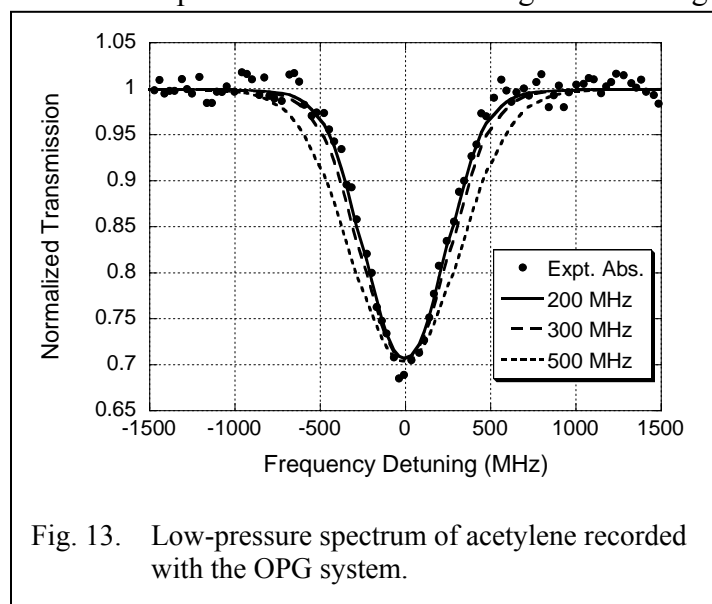Fig. 12 OPLS system featuring an optical parametric generator (OPG) and optical parametric amplifier (OPA).
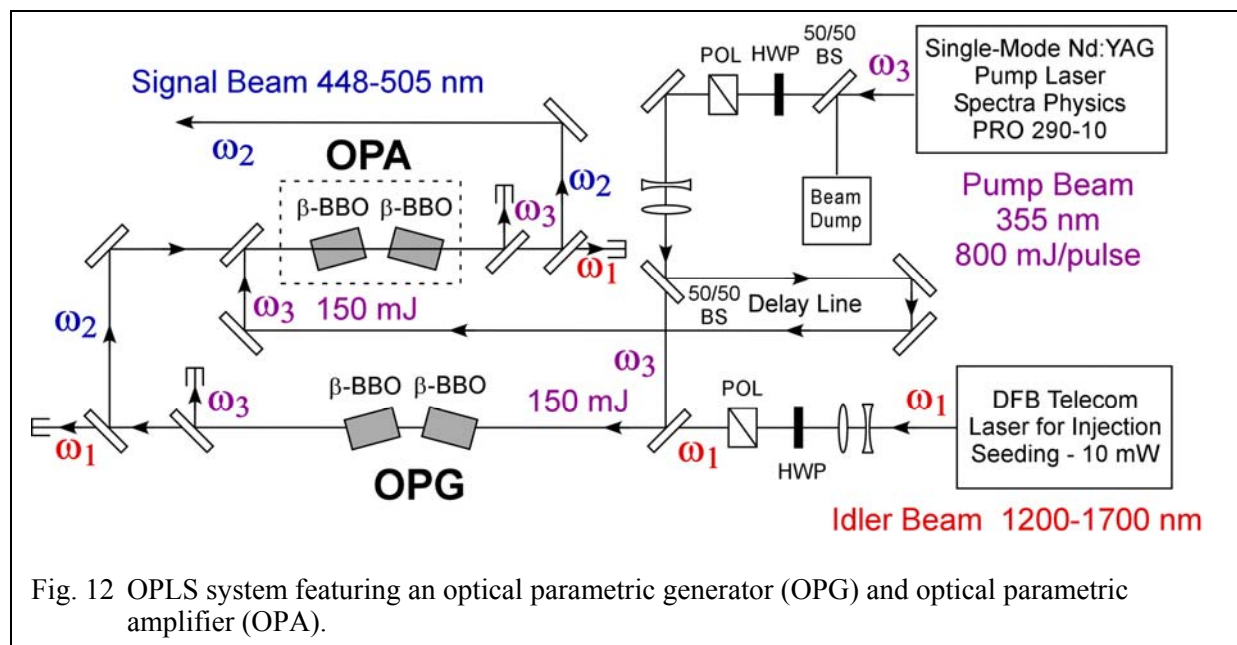
Nd:YAG laser is a Spectra-Physics Model 290-10 optimized for the pumping of optical parametric systems. The BBO crystal is pumped with 100-150 mJ of 355-nm laser radiation. The pump pulse is approximately 8 nsec in duration and the pump beam diameter is approximately 5 mm in the β-BBO crystal. The β-BBO crystal is 10 mm long and 8 mm square in cross section normal to the beam propagation direction. The DFB diode laser produces approximately 10 mW of SLM output in the spectral region from 1534 nm to 1538 nm.

The optical parametric generator/optical parametric oscillator (OPG/OPA) system is shown in Fig. 12. Four β-BBO crystals are used in the OPG/OPA system. The 355-nm pulse energy for the OPG/OPA system is up to 300 mJ/pulse. This pump beam is divided into an OPG pump beam and an OPA pump beam using a 50% beamsplitter. We have demonstrated a signal pulse energy of approximately 18 mJ/pulse at 461 nm from the OPG/OPA system, although at this point we have not put much effort into optimizing the power output of the system.

The frequency spectrum of the laser radiation from the OPG system was analyzed using a solid etalon at the signal wavelength and by recording the absorption line shape for low-pressure acetylene at the idler wavelength. The solid etalon has a free spectral range (FSR) of 10 GHz and a finesse of approximately 15-20. The focused transmission pattern from the etalon was detected using a back-illuminated CCD camera. The estimated spectral resolution of the etalon is approximately 500 MHz, and this sets an upper limit on the frequency bandwidth of the signal radiation from the OPG. The frequency bandwidth of the idler radiation was measured more accurately by performing absorption measurements for low-pressure acetylene. A 5-cm-long gas cell was filled with acetylene at pressures ranging from 0.13 kPa to 2.67 kPa, and a series of absorption spectra were measured with the DFB laser. Theoretical spectra were fit to the experimental spectra using the resonance Doppler width of 471 MHz and the specified 10 MHz frequency bandwidth of the DFB laser. It was determined that the acetylene lines were essentially fully Doppler broadened at pressures below 0.50 kPa.

Absorption spectra were then recorded using the pulsed idler radiation from the OPG. Theoretical spectra were calculated with different values for the frequency bandwidth of the pulsed idler radiation and compared to the experimental spectra as shown in Fig. 13. The best fit to the experimental spectrum is for the theoretical spectrum with a laser frequency bandwidth of 200 MHz full-width-at-half-maximum (FWHM), although the spectrum with a bandwidth of 100 MHz fits nearly as well. The theoretical spectrum with a bandwidth of 300 MHz is significantly wider than the experimental spectrum, and the theoretical spectrum with a bandwidth of 500 MHz is far too wide. The results of the high-resolution absorption measurements indicate that the frequency bandwidth of the idler radiation is 200 MHz or less. The frequency bandwidth of the 1064-nm output of the Q-switched Nd:YAG laser is listed as 100 MHz in the laser specification sheet.

An optical parametric oscillator (OPO) system was also demonstrated. The OPO cavity was formed by placing flat mirrors with reflectivities of 100% and 70% around the OPG stage. The mirrors provide feedback at the signal wavelength but transmit the idler wavelength. The cavity is still not locked to a resonant signal frequency, greatly simplifying tuning compared to locked-cavity systems [8]. However, as is confirmed by absorption measurements of low-pressure acetylene, the frequency spectrum of the laser radiation is still determined by the injection-seeding process and the bandwidth of the laser radiation is not increased by the feedback at the signal beam wavelength provided by the high-reflectivity mirrors. The OPO output is also considerably more intense than the OPG output.

Fig. 13.   Low-pressure spectrum of acetylene recorded with the OPG system.

The major disadvantage of the OPG and OPO laser systems described here compared to commercial dye lasers and OPO systems is the limited wavelength coverage of the DFB-seeded systems. Near infrared DFB lasers that are compatible with our laser driver and control electronics are available at wavelengths from 1200 nm to 1700 nm from NEL, Inc. We have acquired two of these lasers recently, at 1312 nm and 1654 nm for the generation of signal output at 486 nm and 452 nm, respectively. The signal beams at 486 nm and 452 nm will be frequency doubled and used for H-atom LIPS measurements and NO LIF measurements, respectively. These lasers will be plugged into the same driver socket that is used for our 1535 nm laser. Because these DFB lasers are fiber-coupled, the system will not have to be re-aligned when we replace the DFB seed laser.

V. DOE/BES PROJECT PUBLICATIONS 2000-2004

1. T. A. Reichardt, W. C. Giancola, and R. P. Lucht, "Experimental Investigation of Saturated Polarization Spectroscopy for Quantitative Concentration Measurements," *Applied Optics* **39**, 2002-2008 (2000).
2. W. C. Giancola, T. A. Reichardt, and R. P. Lucht, "Multi-Axial-Mode Laser Effects in Polarization Spectroscopy," *Journal of the Optical Society of America B* **17**, 1781-1794 (2000).
3. T. A. Reichardt, F. Di Teodoro, R. L. Farrow, S. Roy, and R. P. Lucht, "Collisional Dependence of Polarization Spectroscopy with a Picosecond Laser," *Journal of Chemical Physics* **113**, 2263-2269 (2000).
4. J. Walewski, C. F. Kaminski, S. F. Hanna, and R. P. Lucht, "Dependence of Partially Saturated Polarization Spectroscopy Signals on Pump Intensity and Collision Rate," *Physical Review A* **64 (6)**, 3816-3827 (2001).
5. S. Roy, R. P. Lucht, and T. A. Reichardt, "Polarization Spectroscopy Using Short-Pulse Lasers: Theoretical Analysis," *Journal of Chemical Physics* **116 (2)**, 571-580 (2002).
6. S. Roy, R. P. Lucht, and A. McIlroy, "Mid-Infrared Polarization Spectroscopy of Carbon Dioxide: Experimental and Theoretical Investigation," *Applied Physics B* **75**, 875-882 (2002).
7. R. P. Lucht, S. Roy, and T. A. Reichardt, "Calculation of Radiative Transition Rates for Polarized Laser Radiation," *Progress in Energy and Combustion Science* **29**, 115-137 (2003).
8. S. F. Hanna, W. D. Kulatilaka, Z. Arp, T. Opatrný, M. O. Scully, J. P. Kuehner, and R. P. Lucht, "Electronic-Resonance-Enhanced (ERE) Coherent Anti-Stokes Raman Scattering (CARS) Spectroscopy of Nitric Oxide," *Applied Physics Letters* **83**, 1887-1889 (2003).
9. W. D. Kulatilaka, R. P. Lucht, S. F. Hanna, and V. R. Katta, "Two-Color, Two-Photon Laser-Induced Polarization Spectroscopy (LIPS) Measurements of Atomic Hydrogen in Near-Adiabatic, Atmospheric Pressure Hydrogen/Air Flames," *Combustion and Flame*, accepted for publication (2004).
10. W. D. Kulatilaka, T. N. Anderson, T. L. Bougher, and R. P. Lucht, "Development of an Injection-Seeded, Pulsed Optical Parametric Generator for High-Resolution Spectroscopy," *Applied Physics B*, submitted for publication (2004).
11. S. Roy, T. B. Settersten, B. D. Patterson, R. P. Lucht, and J. R. Gord, "Two-Color, Two-Photon Laser-Induced Polarization Spectroscopy (LIPS) of Atomic Hydrogen Using Picosecond Lasers," *Physical Review Letters*, submitted for publication (2004).

VI. GRADUATE DISSERTATIONS RESULTING FROM BES SUPPORT 2000-2004

1. Sherif F. Hanna, "Investigation of Pump Polarization Effects on Polarization Spectroscopy in Atmospheric Pressure Flames," M.S. Thesis, Texas A&M (2001).
2. Sukesh Roy, "Application and Development of Advanced Laser Diagnostics for Flame Measurements," Ph.D. Thesis, Texas A&M University (2002).
3. Waruna D. Kulatilaka, "Investigation of Polarization Spectroscopy for Detecting Hydrogen Atom in Flames," M.S. Thesis, Texas A&M University (2002).

VIi. REFERENCES

1   E. V. Baklanov and V. P. Chebotaev, *Optics Communications* **12**, 312 (1974).
2   W. D. Kulatilaka, R. P. Lucht, S. F. Hanna, and V. R. Katta, "Two-Color, Two-Photon Laser-Induced Polarization Spectroscopy (LIPS) Measurements of Atomic Hydrogen in Near-Adiabatic, Atmospheric Pressure Hydrogen/Air Flames," *Combustion and Flame*, accepted for publication (2004).
3   S. Roy, T. B. Settersten, B. D. Patterson, R. P. Lucht, and J. R. Gord, "Two-Color, Two-Photon Laser-Induced Polarization Spectroscopy (LIPS) of Atomic Hydrogen Using Picosecond Lasers," *Physical Review Letters*, submitted for publication (2004).
4   S. F. Hanna, W. D. Kulatilaka, Z. Arp, T. Opatrný, M. O. Scully, J. P. Kuehner, and R. P. Lucht, *Applied Physics Letters* **83**, 1887-1889 (2003).
5   W. D. Kulatilaka, T. N. Anderson, T. L. Bougher, and R. P. Lucht, "Development of an Injection-Seeded, Pulsed Optical Parametric Generator for High-Resolution Spectroscopy," *Applied Physics B*, submitted for publication (2004).
6   W. C. Giancola, T. A. Reichardt, and R. P. Lucht, *Journal of the Optical Society of America B* **17**, 1781-1794 (2000).
7   J. W. Thoman and A. McIlroy, *Journal of Chemical Physics* **104**, 4953-4961 (2000).
8   G. W. Baxter, M. A. Payne, B. D. W. Austin, C. A. Halloway, J. G. Haub, Y. He, A. P. Milce, J. F. Nibler, and B. J. Orr, *Applied Physics B* **71**, 651-663 (2000).